PAPER

Check for updates

Integrated synergy: PSF/PANI/GO membranes for dual-action textile dye detoxification†

Anila Tabasum,‡[a] Amna Siddique,‡[a] Humaira Razzaq, [iD] *[a] Hafiza Hifza Nawaz,[b] Shumaila Razzaque,[c] Saba Tahir, [iD] [a] Shaista Taimur,[a] Nusrat Jabeen[a] and Samreen Shehzadi[d]

The current study addresses the challenge of dye contamination in textile wastewater by developing innovative hybrid polymeric membranes with dual adsorption and filtration capabilities. Through the integration of polyaniline (PANI) into the poly sulfone (PSF) matrix *via* the phase inversion method, a composite membrane was fabricated. Balancing the PANI concentration was crucial, as exceeding 2 wt% led to membrane brittleness and reduced mechanical strength. To address this, the graphene oxide (GO) concentration was optimized. This optimization enhanced the mechanical properties of the nanocomposite membrane. Nanocomposite membranes were well characterized for structural and chemical properties. Batch adsorption studies with MB revealed pseudo-second order kinetics and Langmuir isotherms. The ternary nanocomposite membranes (TCM) exhibited improved water permeability (100 to 534 L m^{-2} h^{-1}), showcasing enhanced filtration capacity. TCM demonstrated a high flux recovery ratio, effectively removing 98% of 70 mg L^{-1} dye at 0.1 MPa. The optimized TCM was successful in filtering real wastewater samples from the Faisalabad textile industry, demonstrating its potential for practical dye removal.

1. Introduction

The release of dye-infused effluents in wastewater from textile industries is an issue of paramount importance that demands immediate attention due to its profound impact on the health of living organisms.[1] According to an estimate, approximately 10–20% of dyes are discharged into freshwater sources as by-products during dyeing application processes.[2] Because even trace amounts of these dyes can be lethal, the task of removing them from wastewater is exceptionally challenging.[2] Simple conventional water treatment methods such as bleaching, electrochemical techniques and photo-degradation are insufficient for the effective removal of dyes from wastewater. Due to the resilience of complex dye molecules to sunlight and aerobic digestion, adsorption has proven to be an efficient

method for their removal. This approach is favored for its environmentally friendly nature and straightforward operational requirements.[3] Despite the advantages of the adsorption process, it still possesses certain limitations, notably in separating and recovering powdered adsorbents.[4] The recovery of these powder adsorbents is energy-intensive, requiring procedures such as high-speed centrifugation or subsequent filtration.[5] Moreover, the continuous removal of impurities from powdered loaded adsorbents in packed columns demands high pressure, leading to elevated energy consumption requirements to maintain water flux.[6] Hence, the pursuit of adsorbents capable of facilitating a continuous and energy-efficient removal process becomes essential. To address this challenge effectively, a more promising approach involves integrating adsorbent materials into the formulation of membrane-forming polymers. This strategy aims to resolve issues related to the separation of adsorbents while also enhancing water permeability. This method is regarded as environmentally benign due to its minimal environmental impact and is highly efficacious in the separation of organic compounds and microorganisms.[7]

At present, among numerous membrane-forming polymers, including polysulfone, polystyrene, polyether sulfone, and poly-vinylidene difluoride polysulfone (PSF), polysulfone has garnered considerable interest in the field of membrane science.[8] The exceptional properties of polysulfone, such as its chemical

[a] Department of Chemistry, University of Wah, Quaid Avenue, Wah Cantt-47040, Pakistan. E-mail: humaira.razzaq@uow.edu.pk

[b] Department of Materials, University of Manchester, Oxford Road, Manchester, M13 9PL, UK

[c] Institute of Physical Chemistry, Polish Academy of Sciences, Kasprzaka 44/52, 01-224 Warsaw, Poland

[d] Central Analytical Facility Division, Pakistan Institute of Nuclear Science & Technology, Islamabad, Pakistan

† Electronic supplementary information (ESI) available. See DOI: https://doi.org/10.1039/d4ma00165f

‡ Equal contribution.

inertness, mechanical strength, thermal stability, and pH resistance, confer significant advantages for membrane fabrication.[9] The hydrophobic nature of PSF dramatically decreases the water flux due to rapid membrane fouling, and acts as a barrier in membrane applications. The development of hydrophilicity in the membrane during the fabrication process, by the addition of a specific adsorptive material, leads to the induction of two functions. This approach may offer dual benefits and holds immense promise for advanced membrane technologies. Addition of adsorptive fillers can enhance the hydrophilic characteristic of PSF membranes by modification methods, such as grafting, surface coating and physical blending in the membrane casting solution.[10] The excessive adsorptive sites and surplus surface area of the adsorbents enhance the efficiency of these membranes. In our previous studies, we studied the adsorptive properties of the hydrophilic polymer PANI and its derivatives for the removal of textile dyes.[11] The potential use of polyaniline (PANI) as an additive to increase the hydrophilicity of the composite membrane is due to the presence of active amines and imines, which show interactions with the pollutants present in wastewater. Fan et al. incorporated polyaniline nanofibers in polysulfone (PSF) membranes, and revealed that the nanocomposite membranes of PSF/PANI exhibited elevated membrane porosity and a well-connected network of membrane pores in comparison to the pristine polysulfone membrane.[12] The addition of PANI in the PSF membrane imparts better adsorption characteristics and increased hydrophilic properties, while an increase in the PANI concentration may cause brittleness, lower mechanical strength, and rapid membrane fouling.[13] The strategic integration of carbon-based materials (out of many other inorganic fillers) into these PANI-modified PSF membranes efficiently deals with these limitations.[14] Targeting the antifouling, mechanical strength and adsorption properties of membranes by carbon-based materials has been validated to yield multifaceted advantages.[15] H. Nawaz et al. fabricated PANI/GO-blended membranes in PVDF through the phase inversion method with enhanced porosity, decreased fouling, high flux rate and better filtration properties.[16] Yun et al. studied polysulfone (PSF) blended with oxidized MWCNTs to develop a composite membrane for BSA removal and water flux increase from 60% to 100%. These membranes were employed to separate dyes and organic pollutants[17] from the water, owing to the good hydrophilicity and improved fouling resistance. Mahendra et al. developed PSF/TiO$_2$/GO nano composite membranes to remove humic acid.[18] Xue Yang et al. fabricated a CNC/PSF blended membrane with improved mechanical strength, thermal stability, and anti-fouling property.[19] The polymer nanocomposite membranes employed in earlier research studies are outlined in Table 2, demonstrating their efficacy in eliminating diverse contaminants from wastewater through adsorptive and filtration properties.

The combination of PANI and GO can significantly enhance the adsorption capacity of the membrane by providing additional active sites for dye molecules. In previous studies, Ali Khan et al. showed that the blending of hydrophilic PANI with inorganic GO results in excellent adsorption due to the presence of effective steric hindrance, and the availability of hydrophilic and active functional groups.[1] This composite shows promise in significantly improving the adsorption and filtration properties of hydrophobic polymers. This interaction not only enhances the structural stability of the membranes, but also improves their mechanical integrity. Additionally, the synergistic effects of PANI/GO improve the membrane selectivity, ensuring the effective removal of targeted contaminants with improved flux.

Owing to the beneficial properties of the nanofiller PANI/GO, their incorporation in PSF resulted in an adsorptive membrane that combines the adsorption and filtration mechanism into one separation process.[20–23]

To the best of our understanding, the current research represents a foremost attempt in highlighting the concerted approach of a tri-component membrane composed of PSF/PANI/GO, indicating a significant advancement in membrane technology specifically tailored for the removal of textile dyes. The primary goal of this research endeavor was to address the issue of membrane brittleness, enhance its anti-fouling properties, s and create a dual-function membrane. The phase inversion method was used for the efficient removal of dyes from both real and simulated samples.

Polyaniline (PANI) in ternary composite membrane materials may undergo intermolecular interactions with certain dye molecules, leading to the chemisorption of dyes. Synergistic effects between PSF, PANI, and GO enhance the capabilities for dye removal. The material effectively captures and removes dye molecules from wastewater, thereby reducing the dye concentration and making the wastewater suitable for discharge or reuse.

The structural and morphological attributes of the membranes were thoroughly examined using techniques, including SEM (scanning electron microscopy), AFM (atomic force microscopy), XRD (X-ray diffraction), and FTIR (Fourier-transform infrared spectroscopy). Furthermore, the mechanical and thermal properties of the developed membranes were assessed via UTM (universal testing machine) measurements and TGA thermogravimetric analysis, respectively. The overall performance and efficiency of the newly developed nanocomposite membrane were assessed by measuring its ability to reject MB, treating real textile wastewater samples, determining volumetric flux, and assessing its fouling reduction capabilities.

2. Experimental

2.1. Chemicals

Polysulfone (PSF) (Sigma-Aldrich/average molecular weight 80 000 g mol^{-1}, density 1.24 g mL^{-1} at 25 °C), graphite-powder (Sigma-Aldrich), aniline (ANI) (Sigma-Aldrich), chloroform (CHCl$_3$) (Sigma-Aldrich), potassium permanganate (KMnO$_4$) (Sigma-Aldrich), ammonium persulfate (APS) (Sigma-Aldrich), 1-methyl-2-pyrolidene (NMP) (Sigma-Aldrich/molecular weight 99.13 g mol^{-1}, density 1.030 g mL^{-1} at 25 °C, bp 202 °C), acetic acid (CH$_3$COOH) (Sigma-Aldrich), sulfuric acid (H$_2$SO$_4$)

(Sigma-Aldrich), sodium dodecyl sulfate (SDS) (Sigma-Aldrich), MB (Sigma-Aldrich), sodium hydroxide (NaOH) (Fisher scientific), propanol (C_3H_8O) (Sigma-Aldrich), ethanol (C_2H_5OH) (Sigma-Aldrich), hydrogen peroxide (H_2O_2) and sodium nitrate ($NaNO_3$) (Sigma-Aldrich) were used.

2.2. Graphene oxide (GO) synthesis

The modified Hummer's approach was used for the synthesis of GO graphene oxide.[24,25] Initially, 200 ml of H_2SO_4 (sulfuric acid), 2.5 g of $NaNO_3$ (sodium nitrate) and 5 g of graphite powder were added to a flask while it was continuously stirred to produce graphite oxide. Later, the suspension-containing flask was gradually filled with 30 g of potassium permanganate and kept in an ice bath at 5–6 °C for 30 minutes. This suspension was kept at 36 °C for an hour, and then distilled water (200 ml) was added at 98 °C. The resultant brown color mixture was further diluted with 500 ml of DI H_2O and oxidized with 30 ml of 10% H_2O_2. The mixture turned from brown to vibrant yellow. After centrifuging the suspension, a thick, yellowish-brown paste was produced. The filtration and washing of the mixture was then followed by drying at 59 °C.

2.3. Synthesis of polyaniline (PANI)

Polyaniline was synthesized through emulsion polymerization by dissolving the aniline monomer in 50 ml of the organic solvent chloroform in the presence of a surfactant (sodium dodecyl sulfate, SDS). Ammonium persulfate (APS) was employed as the oxidant in the reaction. During the synthesis procedure, 0.02 mmol (1.86 mg) of aniline was mixed with 0.4 mmol of SDS (0.115 g) in 50 ml chloroform at 25 °C under continuous stirring. Following this, 0.05 M APS was added dropwise to a mixture solution containing 2 M H_2SO_4. After 30 minutes, the solution exhibited a distinctive green color, signifying the formation of emeraldine salt. The resultant green polyaniline precipitates were purified through acetone washing, dried, and subsequently stored for further analysis.[26]

2.4. Fabrication of the PSF/PANI/GO composite membranes

Seven formulations with different weight proportions of PANI/GO in polysulfone membranes were used. PANI and GO were good candidates to impart hydrophilicity, flux, and improved fouling resistance.[27] For the pure PSF membrane, PSF (14 wt%) was mixed in solvent NMP at 60 °C for some hours, and a homogenous solution was obtained for membrane casting. PANI and GO were added as nano fillers to improve the fouling resistance and hydrophilicity of the pure PSF membrane. Initially, binary composite membranes (PSF/PANI) were casted with varying 11–14 wt% concentrations of PSF, as well as 1–3 wt% concentration of PANI. The 2 wt% addition of PANI was found to be good in binary composite membranes with better preparation and filtration properties. Furthermore, an increase in the amount of polyaniline in the casting solution results in a brittle membrane. For further improvement in the hydrophilicity and antifouling property, ternary composite membranes (PSF/PANI/GO), PSF (11–10 wt%), PANI (2 wt%), and GO (0.5–2 wt%) were used. A ternary composite membrane with PANI 2 wt% and GO

Table 1 Composition of the pristine PSF, PSF/PANI and PSF/PANI/GO composite membranes

Membrane codes	PSF (wt%)	PANI (wt%)	GO (wt%)	NMP (wt%)
P Pristine PSF	14	0	0	86
Pp2g0.5	11.5	2	0.5	86
Pp2g1	11	2	1	86
Pp2g1.5	10.5	2	1.5	86

1 wt% was found to be best for fabrication and application in filtration. By further increasing the amount of GO in the casting solution, the membrane becomes brittle. Then, the membrane casting liquid mixture was carefully poured onto a Petri dish and submersed in a water bath at 25 °C. Subsequently, the membranes were immersed in deionized water to remove any remaining solvent, and then dried at 25 °C. Table 1 presents the composition and Table S2 (ESI†) codes of the PSF-based membranes, while the schematic representation of the phase inversion method is depicted in Fig. 1 below.

2.5. Characterization

Characterization techniques, such as scanning electron microscopy (SEM), atomic force microscopy (AFM), X-ray diffraction (XRD), Fourier transform infrared spectroscopy (FTIR), and thermogravimetric analysis (TGA), were employed in this study. The pH of the MB solution was measured using a digital pH meter (pH master dynamica). FTIR spectroscopy (ALPH 1 Bruker) in the spectral range of 400 to 4000 cm^{-1} was utilized for the analysis of functional groups in GO, PANI, and PSF. XRD analysis of fillers and composite membranes was conducted using a JEOL JDX-3532 X-ray diffractometer (JEOL, Tokyo, Japan) with Cu Kα radiation to provide crystallographic structure information. Morphological studies of PSF, PANI, GO, PSF/PANI, and PSF/PANI/GO were carried out through scanning electron microscopy using a JSM5910 instrument (JEOL, Tokyo, Japan). Thermogravimetric analysis (Diamond series TG/DTA PerkinElmer, USA) was employed to determine the thermal stability of the synthesized PANI, GO, and fabricated membranes in the temperature range of 40–800 °C. The mechanical strength of the composite membranes was assessed using a universal testing machine (UTM, LLOYD Instrument). Surface roughness analyses of composite membranes were conducted using atomic force microscopy (AFM) with a Nanosur Mobile scanning probe optical microscope (Switzerland).

2.6. Membrane performance/stability tests

2.6.1. Porosity. Membranes were cut into 1 cm^2 pieces and placed in deionized water for 24 hours. The membrane weight was measured before and after soaking in water.[27]

The equation for calculating the porosity is as follows:

$$\text{Porosity \%} = \frac{w_2 - w_1/\rho w}{w_{1/\rho w}(w_2 - w_1)/\rho w} \times 100 \qquad (1)$$

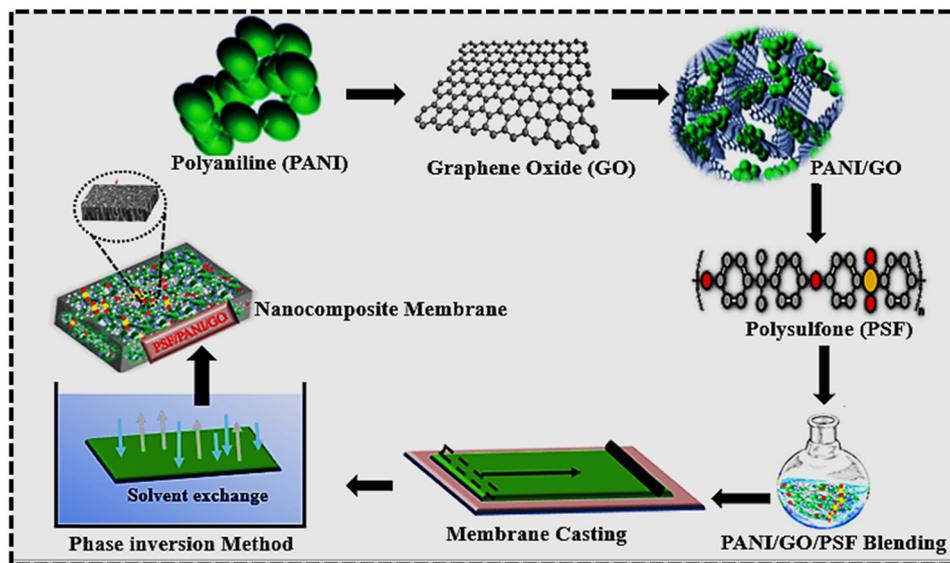Dry membrane weight = W_1, wet membrane weight = W_2, water density = ρw.

Fig. 1 Schematic representation of the PANI/GO/PSF ternary nanocomposite membrane by phase inversion process.

2.6.2. Solvent content. A 1-cm^2 piece of the membranes was dipped in solvents (such as water, methanol, ethanol, and propanol) for 24 h. Then, the membrane weight was determined before and after dipping in the solvents.[28]

The equation for calculating the solvent content is as follows:

$$\text{Solvent content \%} = \frac{W_2 - W_1}{W_2} \times 100 \quad (2)$$

W_1 = weight of dry membrane, W_2 = weight of wet membrane.

2.6.3. Shrinkage ratio. The membrane length and thickness were noted by vernier caliper/screw gauge before and after soaking in water. The following equation is used for the determination of the shrinkage ratio.

$$\text{Shrinkage ratio \%} = \left[1 - \frac{(a \times b)}{(a_0 \times b_0)}\right] \times 100 \quad (3)$$

The variables "a" and "a_0" denote the longitudinal dimension of the dry and wet membrane, respectively. "b" and "b_0" refer to the width for the dry and wet membrane, respectively.

Moreover, the chemical stability of the membranes was also evaluated by exposing the membrane to acidic and alkaline solutions.

2.6.4. Pure water flux. For pure water flux measurements of the membrane, a vacuum filtration pump was used. Water permeability measurements of the pure and composite membranes were tested, followed by soaking the membranes in distilled water for 24 h. Subsequently, the extra water was removed from the surface of the membrane, followed by compacting the membrane using 5 L of deionized water under a pressure of 0.1 MPa. The fabricated membrane performance was evaluated by measuring the pure water flux per minute.[29]

An equation for calculating the pure water flux is provided below.

$$\text{Pure water flux } (J) = \frac{Q}{At} \quad (4)$$

Q = permeate volume

t = time, A = membrane surface area in cm^2.

2.6.5. Antifouling property. The antifouling nature of the membranes was tested with the model protein BSA (Bovine Serum Albumin). The pristine and composite membranes were employed for filtering the feed BSA solution (0.8 g L^{-1}) under a pressure of 0.2 MPa for a duration of 40 minutes. The flux recovery ratio was determined by measuring J_{w1} and J_{w2} (L m^{-2} h^{-1}).[29] The formula used for the (FRR) flux recovery ratio is as follows.

$$\text{FRR \%} = \frac{J_{w1}}{J_{w2}} \times 100 \quad (5)$$

J_{w1} = pure water flux

J_{w2} = flux measurement after washing the fouled membrane.

The rejection-% of BSA was obtained by applying the following formula.

$$\%R = \left(1 - \frac{C_p}{C_f}\right) \times 100 \quad (6)$$

C_p represents the concentration of the permeated BSA solution, while C_f denotes the concentration of the feed BSA solution.

2.6.6. Determination of dye rejection. Dyes (MB and real sample) were passed through composite membranes by using a filtration assembly to determine the dye rejection. A UV-Vis spectrophotometer was used for the feed and permeate concentration in solution.

The dye removal is calculated by applying the following formula.

$$\%R = \left(1 - \frac{C_p}{C_f}\right) \times 100 \qquad (7)$$

2.6.7. Adsorption study. The PSF/PANI/GO composite membrane's adsorption efficiency was investigated during the adsorption experiments toward the model cationic dye (MB). The studies were carried out in 100 ml beakers containing 45.0 ml of MB dye solution and 0.5 g of PSF/PANI/GO composite membranes.

In an isothermal water bath, the samples were kept at a temperature of 298 K for 90.0 minutes. Dye adsorption experiments were performed for the determination of various parameters, such as pH (3–11), contact time (0–24 h), and influence of dye concentration (MB) (12–100 mg L^{-1}). A UV-Vis spectrophotometer helped in the analysis of the initial and remaining MB concentrations.

The adsorption value was calculated by using following equation[30]

$$\text{Adsorption } (q_e) = \frac{(C_0 - C_t)V}{m} \qquad (8)$$

The initial and equilibrium point concentrations of the MB dye are denoted by C_0 and C_e (mg L^{-1}), respectively, while m is the mass of the composite membrane and V is the volume.

The concentration of the MB solution (50 mg L^{-1}) at the pH range of (3–11) was adjusted using 1 M HCl or 1 M NaOH solutions. Polymeric membranes (0.5 g) were immersed in various concentrations of MB solutions at optimized times for kinetic adsorption studies. The adsorption studies were conducted by ternary composite membranes in the MB dye solution of (50 mg L^{-1}). The experiment was repeated at various temperatures of 298 K, 308 K, 318 K and 403 K. By applying the following equation, the adsorption (q_t) value calculated:

$$\text{Adsorption } (q_t) = \frac{(C_0 - C_t)V}{m} \qquad (9)$$

C_0 and C_t (mg L^{-1}) represent the MB concentrations, while V is the volume and m represents the mass of the composite membranes. The comprehensive results and ensuing discussions can be found in the ESI,† for P, Pp2g0.5, Pp2g1, and Pp2g1.5.

3. Results and discussion

The structural characteristics of the prepared nanofillers including PANI, GO and the nanocomposite of PANI-GO and optimized PSF/PANI nanocomposite membranes were verified through detailed analysis using X-ray diffraction (XRD), Fourier-transform infrared spectroscopy (FTIR), and scanning electron microscopy (SEM) techniques, as depicted in the figures of the ESI.† The characterization details of the ternary nanocomposite membranes are provided below.

3.1. Surface morphological analysis

Morphological analysis of the pristine PSF membrane and the impact of the PANI/GO nanofillers on the surface of the membrane was studied by scanning electron microscopy (SEM).

SEM micrographs in Fig. 2. show the pristine PSF, PSF/PANI and the surface of the nanocomposite membranes containing different concentrations of graphene oxide (Pp2g0.5, Pp2g1, Pp2g1.5). Incorporating graphene oxide into the membrane leads to surface irregularities and roughness. These changes are a result of the formation of pores in the membrane structure, as clearly shown in the SEM (scanning electron microscopy) images. The enhanced intermixing of nanofillers with polysulfone (PSF) is attributed to the surface roughness, improved hydrophilic properties, and increased water flux of the membrane. The inclusion of polyaniline into the PSF led to the nucleation and growth process, enhancing the membrane roughness. Hifza *et al.* (2021) explained that PANI addition to the polymer improves the antifouling properties of the membranes. After optimizing the polyaniline incorporation, adding 2 wt% PANI with 1 wt% GO resulted in increased membrane roughness, accompanied by a higher number of pores.[30]

Membrane geometric analysis was conducted using ImageJ software, aiding in determining the pore size from the SEM images. The measurement of the pore diameter and distribution on the surfaces of these membranes is shown in Fig. 2. It is evident from Fig. 2A that the PSF membrane contains fewer pores, whereas an increase in the pore quantity occurs after the introduction of PANI. Meanwhile, further addition of PANI/GO nanofillers increases the occurrence of better pore formation due to more interconnected channels in the membrane. The average pore diameter also decreased with the addition of PANI and GO. The pure PSF membrane has an average pore diameter of approximately 7–8 μm, which was reduced to 2–3 μm in the case of Pp2. Conversely, in the composite membranes (Pp2g0.5, Pp2g1, Pp2g1.5), the pore diameters measure around 2.5 μm, 0.5 μm, and 0.01 μm, respectively.

The strong chemical interaction and intermixing of the PANI/GO nanofillers in PSF (polysulfone) involve various aspects of chemistry, surface charges, functional groups, and intermolecular interactions. Polyaniline (PANI) is a conducting polymer with a backbone of alternating benzene rings and nitrogen atoms, carrying positive charges in its doped form. Graphene oxide (GO) contains oxygen-containing functional groups (like (OH) hydroxyl, epoxy, and (COOH) carboxyl groups) on its surface. These functional groups can engage in various interactions, such as hydrogen bonding, electrostatic interactions, and covalent bonding with other molecules. In the intermolecular realm, interactions between PANI and PSF involve polar–polar interactions. PANI and GO can form a network structure within the PSF matrix through π–π stacking, electrostatic attraction, hydrogen bonding, and potentially covalent bonding. These interactions collectively enhance the mechanical and hydrophilic properties of the composite material.

A cross-sectional examination of pure membranes was also performed utilizing SEM. Fig. 2 also exhibits the cross-sectional images, illustrating the Pp2 and Pp2g1 composite membranes.
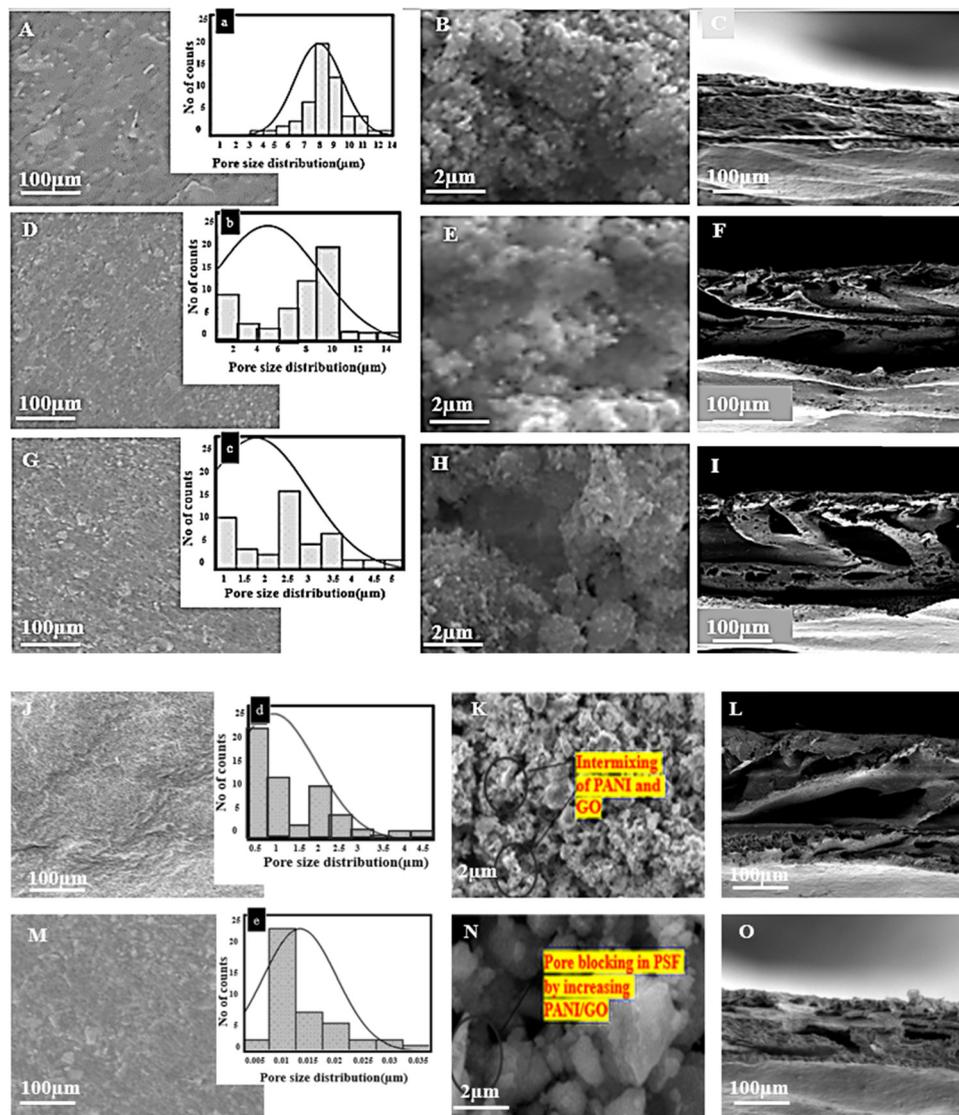
Fig. 2 SEM images of the (A)–(C) surface morphology, pore analysis and cross-sectional image of Pristine PSF P. (D)–(F) Surface morphology, pore analysis and cross-sectional image of Pp2 (PSF: 2 wt% PANI). (G)–(I) Surface morphology, pore analysis and cross-sectional image of Pp2g0.5 (PSF: 2 wt%, PANI: 0.5 wt%GO). (J)–(L) Surface morphology, pore analysis and cross-sectional image of Pp2g1 (PSF: 2 wt%, PANI: 1 wt%GO). (M)–(O) Surface morphology, pore analysis and cross-sectional image of Pp2g1.5 (PSF: 2 wt%, PANI: 1.5 wt%GO).

The exceptional compatibility between the polymers and graphene oxide in the membranes ensures outstanding phase mixing. This cross-section of the membrane exhibits an asymmetric morphology with a thickness of 100 μm.

A dense layer with an asymmetric distribution of pores is revealed in the SEM analysis of the PSF/PANI membrane surface. The surface of the membrane reveals a dense layer of unevenly distributed pores, which from due to rapid phase inversion process of PSF/PANI in the coagulation bath.[31] The uniform distribution of porosity is due to the addition of nanofillers (PANI/GO) within the composite membranes. SEM analysis also shows that the number of pores increases with the addition of filler content. However, more GO may reduce the number of pores due to penetration into the pores. Fig. 2J–L indicates that a filler (GO) content of up to 1 wt% is suitable.

However, further addition of GO causes pore blockage and reduction in the pure water flux of the (Pp2g1.5) membrane.

These SEM images help in the utilization of selective membranes based on their pore sizes for excellent sieving and adsorptive removal of MB dyes. The membrane with the best pore size and flux was selected for AFM analysis.

3D AFM analysis was performed over a specified area of 20 μm × 20 μm to precisely assess the surface roughness of the developed membranes. Fig. 3a–c depicts the results of the AFM analysis on these developed membranes, providing valuable information. In Fig. 3a, the AFM image of the pristine PSF (P) membrane reveals a smooth surface with minimal aggregate formation, indicating the initial state of the membrane. Meanwhile, Fig. 3b illustrates the impact of PANI addition, where the large peaks and valleys on the membrane surface transform
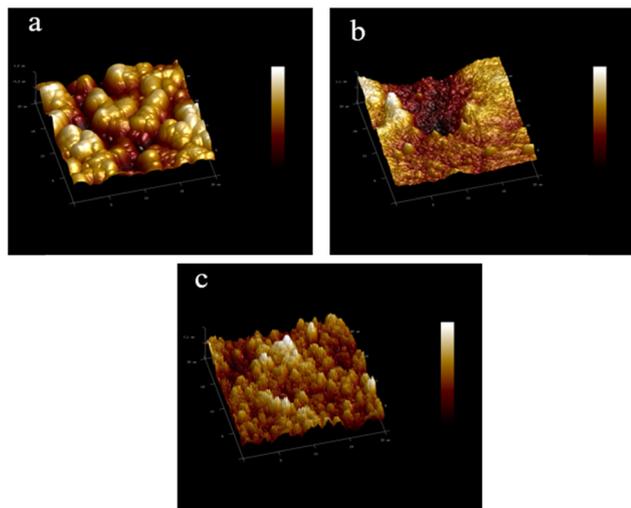
Fig. 3   AFM of (a) P, (b) Pp2, (c) Pp2g1.

into smaller features. This suggests a refinement in the membrane's surface structure due to the incorporation of PANI. Fig. 3c demonstrates the further enhancement in the surface morphology upon the addition of PANI/GO. The presence of PANI/GO leads to an increase in the number of small peaks and valleys on the membrane surface. This phenomenon highlights

the excellent compatibility of GO/PANI with the membrane matrix, resulting in the development of appropriate structures within the membranes.[32]

The increase in the surface roughness corroborated the expansion of the membrane surface area, thereby enhancing the filtration efficiency. Consequently, this surface modification has shown improvement in the membrane antifouling properties, which was attributed to the enhanced porosity, as revealed in SEM images. These findings suggest that the increase in roughness may result in higher water flux and a reduction in the water contact angle. Similar outcomes have been reported in prior research investigations.[30,31]

3.2   Structural, compositional and physiochemical analysis of membranes

The impact of the GO addition with the optimized concentration of PANI was analyzed primarily with FTIR, which confirms the presence of various functional groups on the membrane surface. The FT-IR spectra of PANI and GO are shown in Fig. S3 (ESI†). The FT-IR spectra of the membranes pristine PSF (P), Pp2 and Pp2g0.5, Pp2g1, and Pp2g1.5 composite membranes are shown in Fig. 4a. The pristine PSF spectrum shows peaks at 1160, 1256, 1280, 1350 cm^{-1} and 1400 cm^{-1} for O=S=O, S-O, C-O-C, S-O symmetric, O-S-O asymmetric and aromatic ring, respectively.[33]
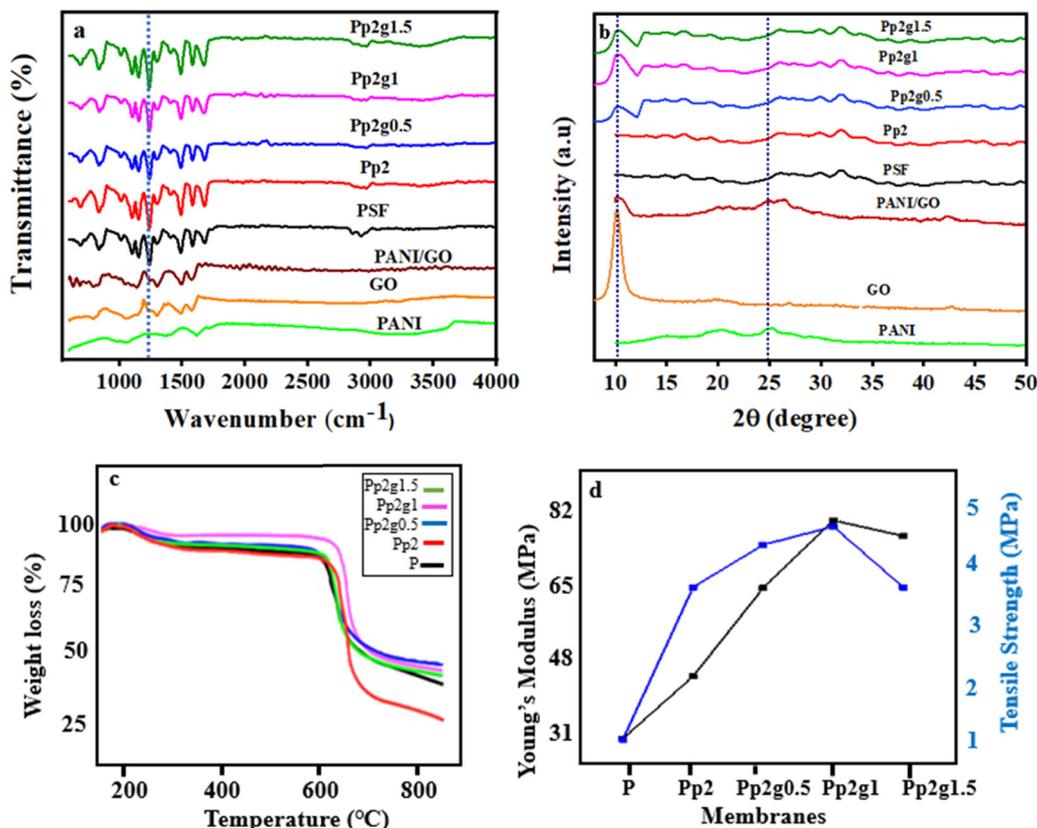

Fig. 4   (a) FTIR spectra of pure PSF, PSF/PANI, and PSF/PANI/GO nanocomposite membranes. (b) XRD diffractogram of PSF, PSF/PANI, and PSF/PANI/GO nanocomposite membranes. (c) TGA of PSF, PSF/PANI, and PSF/PANI/GO nanocomposite membranes. (d) Tensile properties of PSF, PSF/PANI, and PSF/PANI/GO nanocomposite membranes.

Similar peaks in all membranes are due to the presence of the characteristic peaks of PSF. The bands at 800 cm^{-1} and 976 cm^{-1} are assigned to CH_2 and CH out-of-plane vibrations, respectively. The PSF/PANI nano-composite membrane exhibits vibrational bands at 1484 cm^{-1} and 1558 cm^{-1}, corresponding to the benzoid and quinoid groups of polyanilines in the spectrum, respectively. Meanwhile, for the ternary composite membranes (PSF/PANI/GO), graphene oxide characteristic peaks appear at 3428 cm^{-1} for O–H, 1721 cm^{-1} for C=O groups. The ternary composite membranes showed bands at 871 cm^{-1} for the phenyl group, benzoid ring stretching vibration band at 1252 cm^{-1}, and an extra broad peak for N–H bending at 1401 cm^{-1} of polyaniline, suggesting its presence and bonding with PSF. The C–O carbonyl stretching band appearing at 2359 cm^{-1} suggests that each composite membrane has enough GO with OH, COOH to bond with the PSF chain.[33] As the concentration of GO increases, the intensity of the characterization peaks also escalates. This heightened peak intensity is linked to the emergence of intermolecular interaction forces, with a notable emphasis on hydrogen bonding. The increased presence of hydrogen bonding and intermixing in Pp2g1 contributes to the widening of the OH peak at 3428 cm^{-1}. This observation underscores the significant impact of the gradual addition of GO in the PANI/GO/PSF composite membrane. Consequently, it confirms the reduction in the water contact angle attributed to the integration of nanofillers in PSF. This electrostatic interaction between PSF/PANI with GO has excellent interfacial adhesion because the mechanical adhesion also increases, as shown in Fig. 4d.

The XRD analysis presented in Fig. 4b depicts the diffractograms of various samples, including graphene oxide (GO), pure polysulfone (PSF), PANI/GO and PSF/PANI/GO composite membranes. In the case of graphite, two distinct peaks at 26° and 55° corresponding to the (002) and (004) lattice planes, respectively, are expected.[34] Following oxidation, these peaks shift towards smaller angles, indicating changes in the crystal structure. For GO, the diffractogram displays a single peak at 10° corresponding to the (002) plane, confirming the efficacy of the oxidation process. This specific peak at 10° validates the increase in the planar distance between the graphene nanoplatelets due to the introduction of oxygen groups. Consequently, the presence of the $2\theta = 10°$ peak signifies the oxygenated groups in GO, reflecting the augmented interplanar distance.[35] Polyaniline and GO are both amorphous; hence, they will show similar effects individually, as well as in combination.[36] The intensity of the GO peak decreased in the nanocomposite membranes, which confirms the uniform distribution of GO within the composite. As reported by Gascho et al., when GO was vacuum filtered, the XRD pattern started to show peaks other than at 10°, due to partial reaggregation of the graphene oxide.[37] Peaks at lower angles, such as 15°, were generally associated with the presence of amorphous or disordered structures. In the context of the composite studied, this peak suggested the presence of disordered regions. Possibly in PANI or PSF, it indicated an interfacial interaction between GO and the polymer matrix, leading to a disordered arrangement in certain regions of the composite. Regarding the PANI/GO/PSF composite, peaks at 33°–35° were indicative of a specific arrangement or stacking order of the GO layers, possibly influenced by the interactions between GO and the conducting polymer, polyaniline (PANI). The XRD patterns exhibited similar trends across various concentrations of graphene oxide, with only a small shift observed in the position of the hump as the graphene oxide concentration increased.[38,39] The gradual rise in the peak demonstrated the ideal mixing of the PANI/GO/PSF composite, attaining its highest value for Pp2g1. However, the subsequent introduction of more GO led to particle clustering through agglomeration, contributing to the reduction in the peak observed in the case of Pp2g1.5. Considering the SEM observations and the irregular interaction between GO and PSF, a higher concentration of GO could potentially lead to aggregation.

3.3. Thermal and mechanical properties membranes

Thermogravimetric analysis (TGA) was conducted to assess the thermal behavior of pure PSF and composite membranes. Table S4 (ESI†) and Fig. 4c show the thermogravimetric analytical study of pure PSF and nanocomposite membranes. In thermal analysis, pure PSF exhibited swift weight reduction between 180 °C and 500 °C, ascribed to the evaporation of absorbed water. In the case of the PSF/PANI composite membranes (Pp1, Pp2, Pp3), the thermal stability increased from 198 °C to 650 °C.[40] The increase in temperature serves as an indication of the influence of PANI addition on the thermal stability of the composite membranes when compared to pure PSF. Simultaneously, in ternary composite membranes (Pp2g0.5, Pp2g1, Pp2g1.5), the incorporation of GO heightened the thermal stability of the membranes to 690 °C. This aligns with the expectation that the addition of PANI/GO contributes to the improved thermal stability of the composite membrane.[41] The increase in thermal stability can be attributed to substantial electrostatic interactions among PSF, PANI, and GO, facilitated by the presence of functional groups such as OH, NH_2, and COOH, which form interactions with PSF. The maximum degradation temperatures of PSF at 500 °C, Pp2 at 650 °C, and Pp2g1 at 690 °C confirm that the addition of nanofillers enhances the thermal stability of the nanocomposite membranes.[42] Fig. 4d illustrates the evaluation of the mechanical properties of the PSF/PANI/GO nanocomposite membranes using tensile tests. The addition of GO strengthened the nanocomposite membranes in comparison to pure PSF membranes. However, excessive GO addition increased the brittleness.[43] The entanglement of carbon nanoparticles (GO) with the polymeric PSF chain and polyaniline created additional binding sites within the hybrid membrane, fostering strong interactions between the polymer chains and graphene oxide. Consequently, the increase in the GO content elevated the Young's modulus from 36.12 MPa to 78.04 MPa.[44] The significant increase in the surface area of the GO nanosheets played a pivotal role in enhancing their interaction with polymers. Consequently, the tensile strength of the composite membranes was heightened. The mechanical properties of the membranes were enhanced by

the homogeneous miscibility of PANI with GO and PSF in the Pp2g1 composite membrane. The introduction of graphene oxide led to an increase in the tensile strength of polymer nanocomposite membranes, progressing from 0.5 weight percent to 1 wt%. However, adjusting the concentration of GO from 1–1.5 wt% rendered the membranes excessively brittle, leading to easy breakage and subsequently lower tensile strength.[45]

3.6. Membrane permeation properties

Measurements assessed the porosity of diverse nanocomposite membranes,[46] as depicted in Fig. 5a. After the initial weighing, the membranes were immersed in water for a day and re-weighed. The addition of hydrophilic PANI, followed by PANI/GO in PSF, notably increased the membrane porosity, attributed to the introduction of nanofillers creating gaps in the polymer matrix during phase inversion. However, increasing the graphene oxide concentration from 1 wt% to 1.5 wt% reduced the membrane porosity due to potential pore clogging. Incorporating nanoparticles into the membrane increased its thickness due to polymer swelling. For instance, the thickness rose from 100 μm for pristine PSF to 120 μm for Pp2g1.5, with the highest nanoparticle content (Table S3, ESI†). Despite this increase, membrane thickening did not significantly affect the transport resistance. Porosity analysis of the prepared membranes showed that the nanoparticle addition increased the porosity. Pristine PSF had 53% porosity, while the polyaniline

addition increased it to 67%. In the PSF/PANI/GO ternary composite membrane, the GO addition led to porosity increases to 73% for Pp2g0.5 and 81% for Pp2g1. However, in Pp2g1.5, the porosity decreased due to GO nanoparticle agglomeration. Porosity significantly affected the % shrinkage ratio, decreasing with enhanced membrane hydrophilicity. This decrease maintains the pore structures, enhancing the adsorption and antifouling properties. These findings are illustrated in Fig. 5a, showing that the % shrinkage ratio decreases with increasing hydrophilic nanofiller concentration.

Stability studies revealed consistent FTIR results before and after membrane exposure to acid solution and washing, indicating no leaching of PANI or GO, ensuring membrane robustness against strong acidic or basic environments. The successful blending of the PANI/GO/PSF membrane matrix underscores its structural integrity.

Water contact angle measurements were performed to assess the composite membrane hydrophilicity, with lower angles indicating higher hydrophilicity. Fig. 5d shows decreased contact angles (from 84° to 37°) with PANI/GO addition, enhancing the membrane wettability and resistance to fouling. PSF's inherent hydrophobicity is counteracted by PANI's –NH group and GO's functional groups, promoting interactions and facilitating solvent adsorption and filtration.

Solvent absorption tests with four solvents of varying polarity showed that increasing the filler content enhanced the water
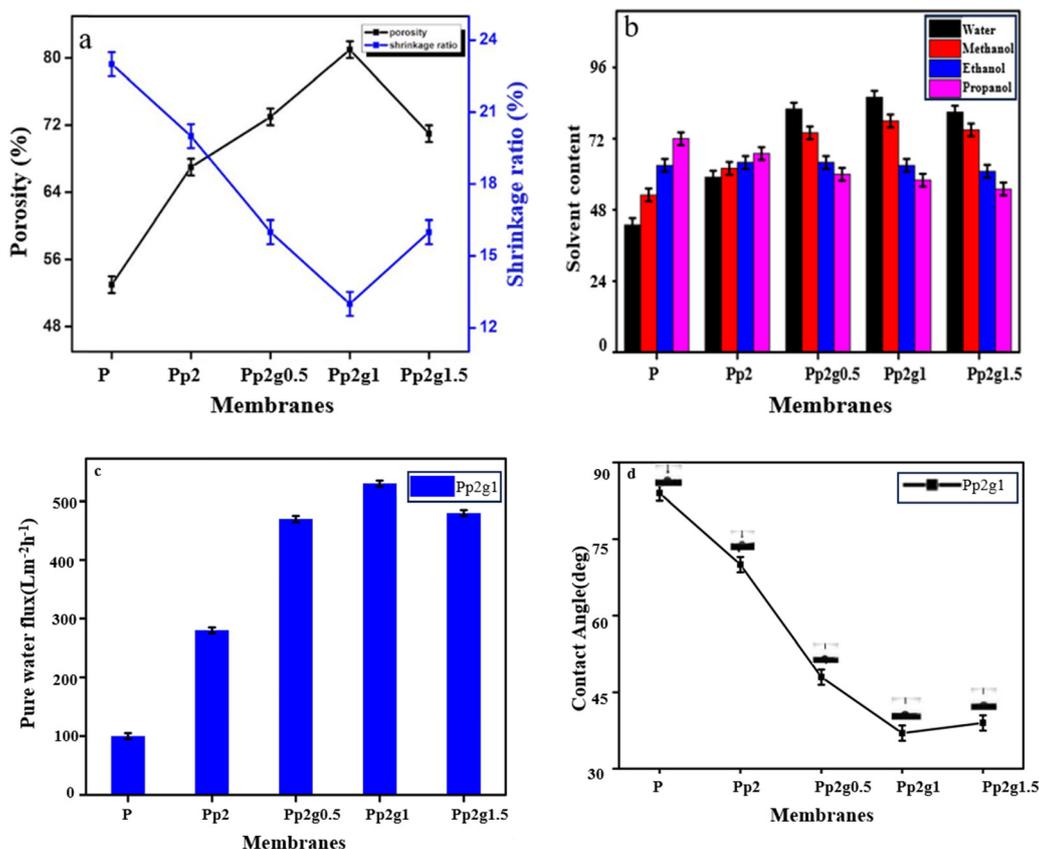

Fig. 5 (a) Porosity and percentage shrinkage ratio, (b) solvent content, (c) (PWF) pure water flux, (d) contact angle.

permeability and hydrophilicity. However, further GO addition induced hydrophobicity due to aggregation, enhancing the anti-fouling and adsorption capabilities.[47–50]

The pure water flux (PWF) for the PSF/PANI membranes, illustrated in Fig. 5c, increased significantly with 0.5 wt% and 1 wt% GO addition, enhancing the water flux rate, adsorption, and filtration abilities. However, increasing the GO percentage (1 wt% to 2 wt%) led to pore blockage and decreased pure water flux.

In short, the heightened porosity and decrease in the water contact angle synergistically promote heightened water flux in Pp2g1. Enhanced porosity facilitates greater water permeability, while decreased contact angle signifies enhanced membrane wettability, thus expediting water passage.

3.7. Antifouling properties and BSA rejection of composite membranes PSF/PANI/GO

The deposition of solute particles during the membrane filtration causes membrane fouling and flux reduction. To overcome the challenge of membrane fouling, the addition of hydrophilic fillers into the membrane is significant. In the current study, incorporation of fillers (PANI/GO) to the casting solution enhanced the hydrophilicity and reduction in fouling. In the filtration studies for composite membranes, a model fouling agent called bovine serum albumin was used. The flux recovery ratio was measured before and after filtration of the feed solution (BSA).[51]

Fig. 6a illustrates a progressive enhancement in the BSA rejection with the incremental incorporation of nanofillers into the hydrophobic PSF membrane. Pristine PSF, owing to its hydrophobic nature, exhibits a relatively low BSA rejection rate of approximately 37%. However, the gradual introduction of PANI at 2 wt% elevates the rejection rate to 60s%, a trend that is further highlighted in the cases of Pp2g0.5 and Pp2g1 membranes, where the rejection rates range from 78% to 85%. Conversely, a slight reduction in rejection is observed with the Pp2g1.5 membrane. This phenomenon can be attributed to the increased concentration of GO, which causes pore reduction, as evidenced by SEM analysis.

The reusability and resistance to fouling of the membranes were evaluated using a MB solution. After each cycle, the fouled membranes were subjected to washing with an ethanol solution for a duration of half an hour before being reused. The antifouling properties were investigated across various membrane compositions, including P, Pp2, Pp2g0.5, Pp2g1, and Pp2g1.5.

Observations revealed a progressive deterioration in the membrane pore integrity with each successive passage of MB, attributable to the adsorption of the dye molecules onto the membrane surface. Consequently, a decline in flux was consistently observed after each cycle, primarily due to pore blockage induced by the dye molecules. However, employing thorough cleaning procedures before each subsequent cycle facilitated favorable recovery and improved flux rates.

The optimized Pp2g1 composition exhibited superior flux recovery compared to other compositions, a trend which was corroborated by AFM water contact angle studies and SEM analysis, demonstrating increased porosity (refer to Fig. 6b). Furthermore, after four cycles, the flux recovery ratio (FRR) of the prepared composite membranes (Pp2, Pp2g1) surpassed that of the pure PSF membrane.[52,53]

Results from BSA rejection experiments underscored the enhanced performance of Pp2g1, attributed to its greater hydrophilicity and negatively charged surface, which facilitates stronger electrostatic repulsion between BSA molecules and the membrane surface, thus reducing flux decline rates.[35,54]

3.8. Proposed mechanism for the rejection of dye and BSA with increased flux

Adsorptive membranes are usually employed to remove dyes from wastewater by dual action: adsorption and rejection. When water-soluble dyes encounter the active layer of the membrane, molecular sieving helps in dye and BSA rejection, where the high molecular weight dye and BSA were rejected by the smaller pores of membranes. Furthermore, the adsorption mechanism is explained by the attractive forces (electrostatic, dipole, van der Waals interactions and hydrogen bonding) between the cationic dye and reactive functional groups like $-NH_2$, OH and $-COOH$ present on the surface of the composite membrane.
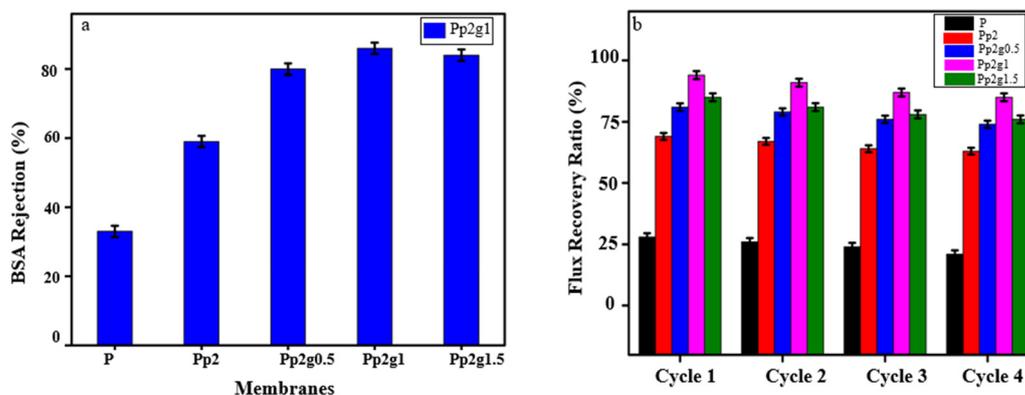

Fig. 6 (a) BSA rejection of pristine PSF P and composite membrane Pp2, Pp2g0.5, Pp2g1, Pp2g1.5. (b) Flux recovery ratio of pristine PSF P and composite membrane Pp2, Pp2g0.5, Pp2g1, Pp2g1.5.

In the current study, the key mechanism of BSA and dye rejection is sieving and electrostatic rejection or adsorption, respectively.

The rejection of BSA (bovine serum albumin) from the small pore size membranes is primarily driven by size exclusion. The small
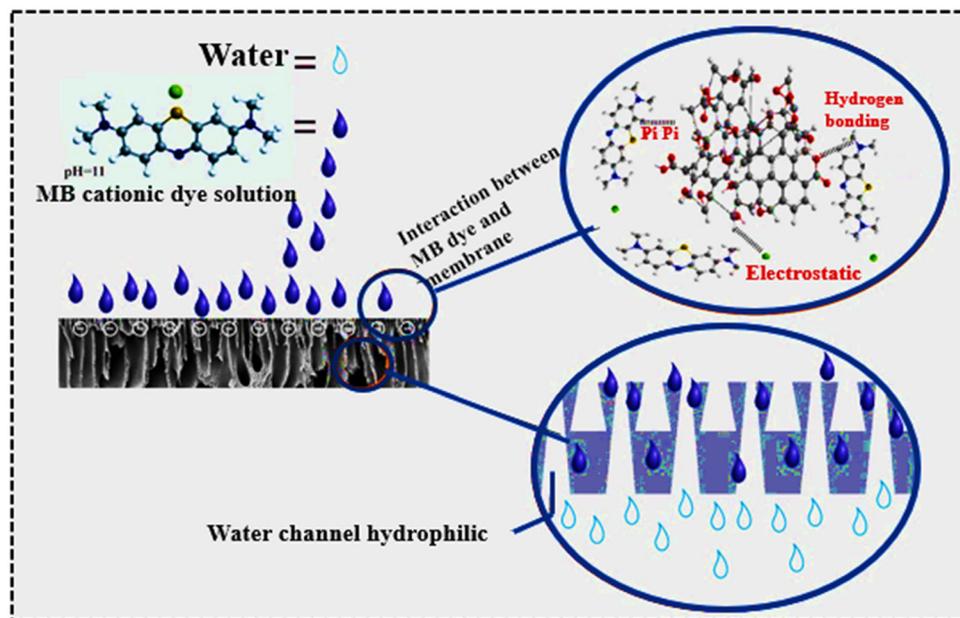

Fig. 7 Proposed diffusion mechanism through the PSF/PANI/GO nanocomposite membranes adsorptive removal of MB dye from a wastewater sample.
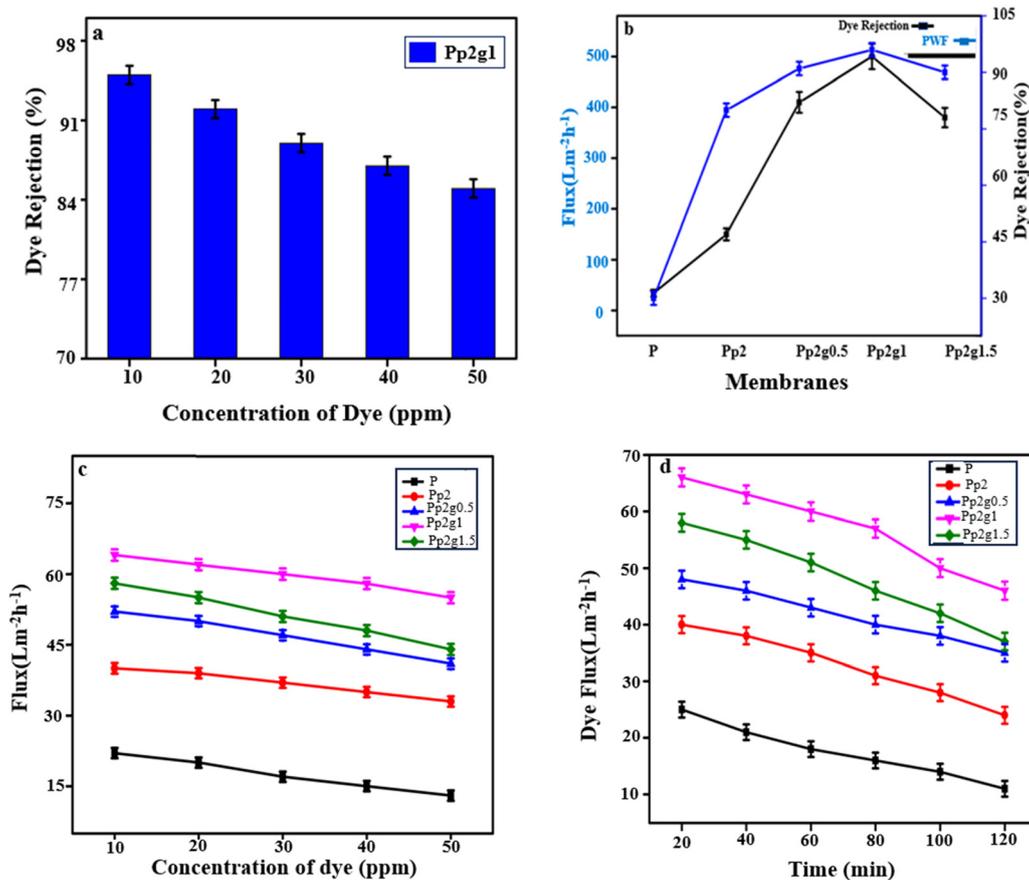

Fig. 8 (a) and (b) dye rejection, (c) and (d) dye flux.

pores restrict the passage of larger molecules such as BSA, allowing only smaller molecules to pass through. This mechanism effectively separates BSA from the filtrate. The passage of the MB dye through a membrane indicated the charge characteristics of the membrane surface. The ease of dye permeation suggested a negative surface charge, attributed to electrostatic interactions. The rejection rate and flux of dyes through membranes depend on the molecular weight of the dye. The pores in the prepared membranes are smaller compared to the size of the MB dye, which measures $17.0 \times 7.6 \times 3.3$ Angstroms. Since the MB dye molecules are relatively large in terms of their hydrodynamic diameter, the sieving or size exclusion process of these dyes through the nanocomposite membranes could be responsible for controlling the flow of contaminated water. In comparison to the pure PSF membrane, the composite membrane made of polysulfone, graphene oxide, and polyaniline exhibited a greater rate of dye rejection of about 98% for MB and 96%, 89% for real samples, respectively. In the adsorption mechanism, the separation of the MB dye from contaminated water is made easier by the electrostatic interactions and

hydrogen bonding between the positively charged nitrogen groups of MB and the carboxyl and hydroxyl groups of GO sheets and the –NH group of PANI. Owing to the adsorptive nature of the porous membranes, all membranes exhibited dye rejection.

Enhanced rejection of dye and BSA can lead to improved flux through a membrane by mitigating fouling and blockage. Effective rejection of these substances prevents clogging of the membrane pores, which can otherwise impede flux. The proposed mechanism, as illustrated in Fig. 7, highlights the synergistic effects of sieving, electrostatic interactions, and adsorption in enhancing the rejection efficiency of membranes, thereby improving the flux rates and overall filtration performance.

3.9 Implication of the dye concentration on the flux and recyclability

The dye concentration in the feed solution plays a very important role in evaluating membrane performance, as stated by the film theory equation.[55,56]
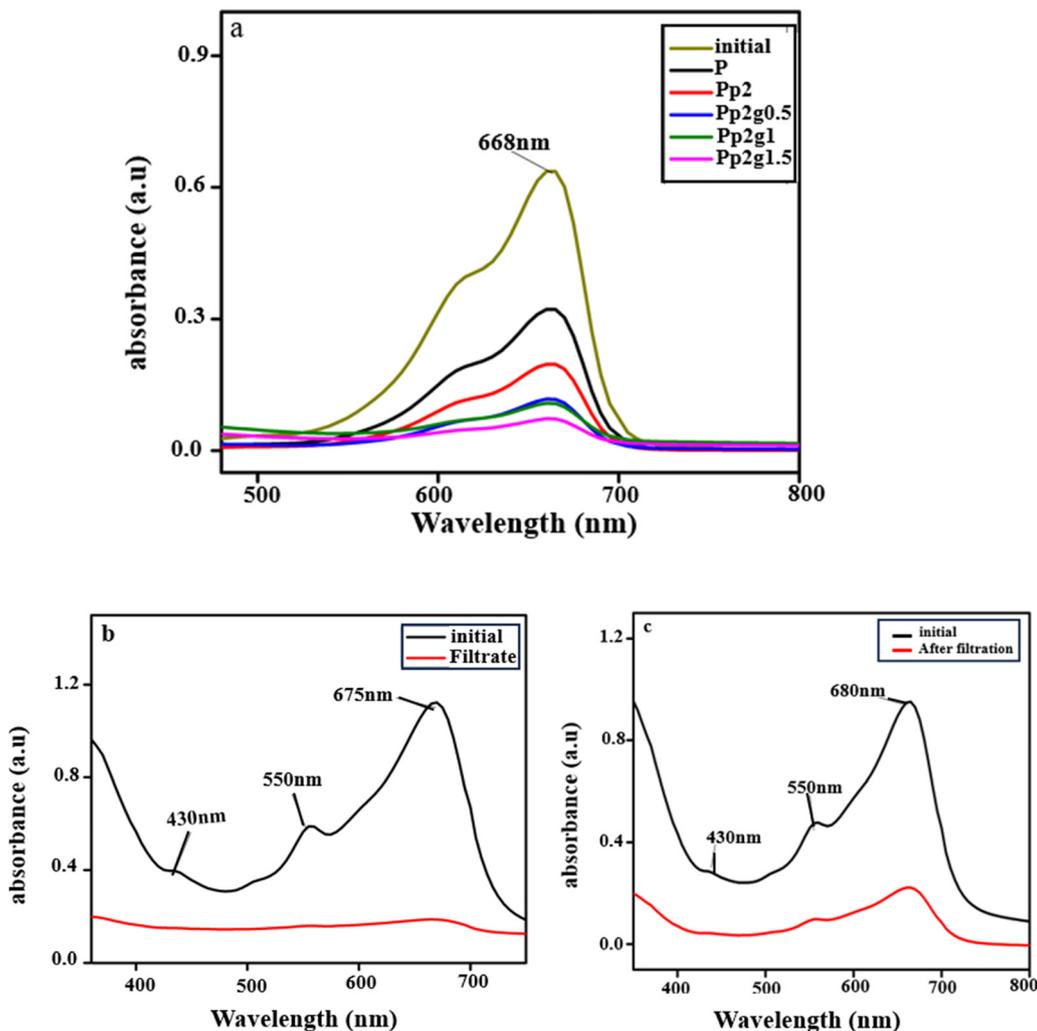

Fig. 9 (a) Removal of the MB dye through composite membranes (P, Pp2, Pp2g0.5, Pp2g1, Pp2g1.5). (b) and (c) Removal of indigo dye and dyes from real samples by using the Pp2g1 composite membrane.

In this study, different concentrations of the MB (10, 20, 30, 40, 50 ppm) were used for the effective determination of the fabricated composite membrane.

Fig. 8(a–d) display the results for dye rejection and water flux, respectively.

These results show that the increase in dye concentrations (from 10 to 50 ppm) caused a decrease in the water flux and dye rejection. The dye molecule aggregation on the membrane surface due to the increase of the dye concentration leads to high osmotic pressure within the membranes. Additionally, dye molecules have influence on the membrane surface porosity through adsorption, which leads to membrane fouling.[57]

On the basis of these obtained results, it can be decided that these ternary nanocomposite membranes (PANI/GO/PSF) have great potential in the field of textile effluent treatment, especially for the removal of dyes.

The recyclability tests demonstrated that the manufactured membranes exhibit excellent durable stability during the nanofiltration process.[58] Consequently, these efficient membranes provided a superior solution for effectively removing dyes from textile effluent. Furthermore, these membranes could be used for the rejection of the dye mixture.

3.10. Real sample analysis

For the determination of practical relevance and applicability of our findings, real textile wastewater samples were collected from the textile industry, Faisalabad Pakistan, to investigate their treatment potential from prepared ternary nanocomposite membranes. Firstly, the sample was contaminated with indigo dye and the second one with a mixture of indigo and black 4 G. After that, the best optimized membrane Pp2g1 was dipped in deionized water for 24 hours to improve its overall efficiency.[59] Then, real textile wastewater samples were passed through this membrane by using a filtration assembly at 0.25 MPa (36.35 Psi) with a time break of 15 minutes between each filtration cycle. Filtration was stopped after passing the selected amount of permeate, then the retentate was emptied and analyzed under UV-Vis spectroscopy. The membranes went under physical cleaning with DI water in a sonication bath for 15 minutes at 250 rpm. Irreversible fouling of the membrane was determined by taking the difference between the permeate and initial water concentration.[60] Color retention was determined by using UV absorbance. Under optimized conditions, filtrate analysis done on Pp2g1 by UV-Vis showed 96% and 89% dye removal from sample 1 and sample 2, respectively. All tests were run three times to ensure reproducibility. The UV study of the MB-saturated permeate solution from pure PSF P and composite membranes Pp2, Pp2g0.5, Pp2g1, Pp2g1.5 is shown in Fig. 9a. An increase in the PANI/GO filler content causes a decrease in the absorbance values of saturated permeate solutions because the nanocomposite membranes were better able to remove the dyes.[61] Due to its small size, the 0.5 μm ternary composite membrane Pp2g1 can be used for nanofiltration of the MB dye. In contrast to the hydrophilic PSF with a higher contact angle (84°), the novel (PSF/PANI/GO) ternary composite membrane Pp2g1, which has a lower contact angle (37°), showed more antifouling tendency. Owing to the findings, ternary composite membranes PSF/PANI/GO have potential for treating textile effluents.[62]

In the future, the practical application of this research work may involve assessing the dye removal capability of this novel ternary PANI/GO/PSF membranes, thereby increasing their competitiveness in the field.

Table 2 A comparative study of earlier research on polymer-based nanocomposite membranes for efficient dye adsorption and filtration

Sr. No.	Fillers	Synthesis method	Membrane properties	Maximum adsorption capacity/filtration pressure	Dye rejection %	Ref.
1	PVDF/GO	Electro spinning/ ultra sonication	Increased in hydrophilicity by decreasing the contact angle from 131.1° to 66.6°	621.1 mg g^{-1}	99%	19
2	Porous regenerated cellulose (RC) membrane	Controlled oxidation reaction technique	Membrane porosity = 72%	403 mg g^{-1} for cationic dye	98%	65
			Water flux = 6.14 L m^{-2} h^{-1} bar^{-1}	139 mg g^{-1} for anionic dye	88%	
			Pore size = 25.9 nm			
3	Ceramic ultrafiltration membrane	Physiochemical treatment	Flux =14.7 and 16.4 L h^{-1} m^{-2} bar	Dye conc. 50 ppm under 3 bars	99%	66
			Pore size = 75–90 nm (pore size)			
4	PVA membranes functionalize by D-glucose and agar	Solution casting method	Water contact angle = 63°	29 mg g^{-1}	99%	67
			Tensile strength (>13 MPa) and high elongation at break (>170%).			
5	Grafted titania pillared clay membranes	Dip coating by colloidal sol–gel route	Contact angle of membrane = 107 ± 1°	30 ppm dye conc. under 12–17 psi	100%	
			Water flux = 70–110 L m^{-2} h^{-1}			68
6	PSF/PANI/GO	Phase inversion method	Contact angle = 84°–37°	Study of adsorption, as well as filtration 70 mg L^{-1}	98% for lab MB sample dye	Current study
			Water flux = 100–534 L m^{-2} h^{-1}	10–200 ppm dye	96% for real sample	
			Thermal stability = 137–614 °C	Concentration under 0.2 MPa		

Recycling assessments indicate that the produced membranes exhibit robust stability over an extended period in the nanofiltration process. Consequently, these pioneering membranes introduce a new approach to eliminate dyes from textile wastewater.[63,64] Under the same settings, the PSF/PANI/GO composite membrane performance was found to be superior to that of known technologies. The ability of the new PSF/PANI/GO composite membranes to remove dye could be improved in the future to increase their competitiveness. Furthermore, a prospective collaboration with industry partners is viable for analyzing genuine water samples, leading to an extended membrane lifespan of 2–4 years.

4. Conclusion

This study focused on improving hydrophobic polysulfone (PSF) membranes by incorporating polyaniline (PANI) and graphene oxide (GO). The best combination was found to be 2 wt% PANI and 1 wt% GO. This modification enhanced the ability of the membranes to filter dyes and adsorb contaminants in a single step.

The key findings are as follows:

1. Ternary composite membranes showed reduced shrinkage and increased surface roughness compared to pure PSF membranes, leading to enhanced adsorption and filtration of dyes.

2. Incorporating GO and PANI increased the hydrophilicity of the membranes, reducing the water contact angle from 84° to 37°.

3. Water flux increased significantly from 100 to 534 L m^{-2} h^{-1}, and the rejection rate for BSA improved from 34% to 84%.

4. The adsorption performance of ternary composite membranes surpassed that of powdered PANI adsorbents and pure PSF, even with real dye samples. The adsorption process followed the Langmuir isotherm and pseudo-second-order kinetic model.

5. The thermal stability of the membranes improved with the addition of PANI and GO, increasing the degradation temperature from 493 °C to 627 °C.

6. Ternary composite membranes exhibited high rejection capacities for the MB dye (98%) and real samples (96%).

These findings suggest that the developed membranes hold promise for the cost-effective removal of dyes from wastewater. Their dual action in adsorption and filtration can improve the water quality and extend the membrane lifespan, making them suitable for practical applications in water treatment.

Data availability

Data will be made available on request.

Conflicts of interest

The authors declare that they have no known competing financial interests or personal relationships that could have appeared to influence the work reported in this paper.

References

1 M. Munir, M. F. Nazar, M. N. Zafar, M. Zubair, M. Ashfaq, A. Hosseini-Bandegharaei, S. U. Khan and A. Ahmad, Effectivess adsorptive removal of methylene blue from water by didodecyldimethylammonium bromide-modified Brown clay, *ACS Omega*, 2020, **5**(27), 16711–16721.

2 Z. W. Heng, Y. Y. Tan, W. C. Chong, E. Mahmoudi, A. W. Mohammad, H. C. Teoh, L. C. Sim and C. H. Koo, Preparation of a novel polysulfone membrane by incorporated with carbon dots grafted silica from rice husk for dye removal, *J. Water Proc. Eng.*, 2021, **40**, 101805.

3 B. Said, S. M'rabet, R. Hsissou and A. El Harfi, Synthesis of new low-cost organic ultrafiltration membrane made from Polysulfone/Polyetherimide blends and its application for soluble azoic dyes removal, *J. Mater. Res. Technol.*, 2020, **9**(3), 4763–4772.

4 Y. Li, Y. Gao, C. Yang, Z. Wang and G. Xue, Facile and controllable assembly of multiwalled carbon nanotubes on polystyrene microspheres, *Chin. J. Polym. Sci.*, 2014, **32**(6), 711–717.

5 E. K. Aziz, R. Abdelmajid, L. M. Rachid and E. H. Mohammadine, Adsorptive removal of anionic dye from aqueous solutions using powdered and calcined vegetables wastes as low-cost adsorbent, *Arab J. Basic Appl. Sci.*, 2018, **25**(3), 93–102.

6 A. Umeno, Y. Miyai, N. Takagi, R. Chitrakar, K. Sakane and K. Ooi, Preparation and adsorptive properties of membrane-type adsorbents for lithium recovery from seawater, *Ind. Eng. Chem. Res.*, 2002, **41**(17), 4281–4287.

7 M. Hui, P. Shengyan, H. Yaqi, Z. Rongxin, Z. Anatoly and C. Wei, A highly efficient magnetic chitosan "fluid" adsorbent with a high capacity and fast adsorption kinetics for dyeing wastewater purification, *Chem. Eng. J.*, 2018, **345**, 556–565.

8 A. L. Gao and Y. Wan, Iron modified biochar enables recovery and recycling of phosphorus from wastewater through column filters and flow reactors, *Chemosphere*, 2023, **313**, 137434.

9 Q. Gui, Q. Ouyang, J. Zhang, S. Shi and X. Chen, Ultrahigh flux and strong affinity poly (N-vinylformamide)-grafted polypropylene membranes for continuous removal of organic micropollutants from water, *ACS Appl. Mater. Interfaces*, 2021, **13**(17), 20796–20809.

10 Z. Fan, Z. Wang, M. Duan, J. Wang and S. Wang, Preparation and characterization of polyaniline/polysulfone

nanocomposite ultrafiltration membrane, *J. Membr. Sci.*, 2008, **310**(1–2), 402–408.

11 R. M. Al-Maliki, Q. F. Alsalhy, S. Al-Jubouri, I. K. Salih, A. A. AbdulRazak, M. A. Shehab, Z. Németh and K. Hernadi, Classification of Nanomaterials and the Effect of Graphene Oxide (GO) and Recently Developed Nanoparticles on the Ultrafiltration Membrane and Their Applications: A Review, *Membranes*, 2022, **12**(11), 1043.

12 J. A. Oyetade, R. L. Machunda and A. Hilonga, Photocatalytic degradation of azo dyes in textile wastewater by Polyaniline composite catalyst-a review, *Afr. J.*, 2022, e01305.

13 A. Khalid, A. Ibrahim, O. C. S. Al-Hamouz, T. Laoui, A. Benamor and M. A. Atieh, Fabrication of polysulfone nanocomposite membranes with silver-doped carbon nanotubes and their antifouling performance, *J. Appl. Polym. Sci.*, 2017, **134**(15), 109569.

14 M. S. A. Wahab, S. Abd Rahman and R. A. Samah, Hydrophilic enhancement of Polysulfone membrane via Graphene Oxide embedded thin film nanocomposite for Isopropanol dehydration, *Vacuum*, 2020, **180**, 109569.

15 A. M. Díez-Pascual, Chemical functionalization of carbon nanotubes with polymers: a brief overview, *Macromol*, 2021, **1**(2), 64–83.

16 P. Semeraro, P. Fini, M. D'addabbo, V. Rizzi and P. Cosma, Agriculture; Biotechnology, Removal from wastewater and recycling of azo textile dyes by alginate-chitosan beads, *Int. J. Environ., Agric. Biotechnol.*, 2017, **2**(4), 238860.

17 H. Zhang, X. Quan, S. Chen, H. Zhao and Y. Zhao, Fabrication of photocatalytic membrane and evaluation its efficiency in removal of organic pollutants from water, *Sep. Purif. Technol.*, 2006, **50**(2), 147–155.

18 M. Duhan and R. Kaur, Nano-structured polyaniline as a potential adsorbent for methylene blue dye removal from effluent, *J. Compos. Sci.*, 2020, **5**(1), 7.

19 F. Ma, D. Zhang, T. Huang, N. Zhang and Y. Wang, Ultrasonication-assisted deposition of graphene oxide on electrospun poly (vinylidene fluoride) membrane and the adsorption behavior, *Chem. Eng. J.*, 2019, **358**, 1065–1073.

20 S. Palaniappan and A. John, Polyaniline materials by emulsion polymerization pathway, *Prog. Polym. Sci.*, 2008, **33**(7), 732–758.

21 L. Eykens, K. De Sitter, C. Dotremont, L. Pinoy and B. Van der Bruggen, Membrane synthesis for membrane distillation: a review, *Sep. Purif. Technol.*, 2017, **182**, 36–51.

22 A. Hussain and M. Al-Yaari, Development of polymeric membranes for oil/water separation, *Membranes*, 2021, **11**(1), 42.

23 A. M. Alosaimi, M. A. Hussein, M. Y. Abdelaal, T. R. Sobahi and H. D. Rozman, Polysulfone/wood flour/organoclay hybrid nanocomposites as efficient eco-friendly materials, *Compos. Interfaces*, 2020, **27**(8), 717–736.

24 H. Nawaz, M. Umar, A. Ullah, H. Razzaq, K. M. Zia and X. Liu, Polyvinylidene fluoride nanocomposite super hydrophilic membrane integrated with Polyaniline-Graphene oxide nano fillers for treatment of textile effluents, *J. Hazard. Mater.*, 2021, **403**, 123587.

25 N. I. Zaaba, K. L. Foo, U. Hashim, S. J. Tan, W. W. Liu and C. H. Voon, Synthesis of graphene oxide using modified hummers method: solvent influence, *Proc. Eng.*, 2017, **184**, 469–477.

26 G. Zhang, M. Zhou, Z. Xu, C. Jiang, C. Shen and Q. Meng, Guanidyl-functionalized graphene/polysulfone mixed matrix ultrafiltration membrane with superior permselective, antifouling and antibacterial properties for water treatment, *J. Colloid Interface Sci.*, 2019, **540**, 295–305.

27 E. N. Zare, A. Motahari and M. Sillanpää, Nanoadsorbents based on conducting polymer nanocomposites with main focus on polyaniline and its derivatives for removal of heavy metal ions/dyes: a review, *Environ. Res.*, 2018, **162**, 173–195.

28 Y. Zhou, J. Lu, Y. Zhou and Y. Liu, Recent advances for dyes removal using novel adsorbents: a review, *Environ. pollut.*, 2019, **252**, 352–365.

29 H. B. Slama, A. Chenari Bouket, Z. Pourhassan, F. N. Alenezi, A. Silini, H. Cherif-Silini, T. Oszako, L. Luptakova, P. Golińska and L. Belbahri, Diversity of synthetic dyes from textile industries, discharge impacts and treatment methods, *Appl. Sci.*, 2021, **11**(14), 6255.

30 P. Bhol, S. Yadav, A. Altaee, M. Saxena, P. K. Misra and A. K. Samal, Graphene-based membranes for water and wastewater treatment: a review, *ACS Appl. Nano Mater.*, 2021, **4**(4), 3274–3293.

31 M. R. Esfahani, S. A. Aktij, Z. Dabaghian, M. D. Firouzjaei, A. Rahimpour, J. Eke, I. C. Escobar, M. Abolhassani, L. F. Greenlee, A. R. Esfahani and A. Sadmani, Nanocomposite membranes for water separation and purification: fabrication, modification, and applications, *Sep. Purif. Technol.*, 2019, **213**, 465–499.

32 S. Hussain, X. Wan, Z. Li and X. Peng, Cu-TCPP nanosheets blended polysulfone ultrafiltration membranes with enhanced antifouling and photo-tunable porosity, *Sep. Purif. Technol.*, 2021, **268**, 118688.

33 A. Samadi, M. Xie, J. Li, H. Shon, C. Zheng and S. Zhao, Polyaniline-based adsorbents for aqueous pollutants removal: a review, *Chem. Eng. J.*, 2021, **418**, 129425.

34 Z. Rahimi, A. A. Zinatizadeh, S. Zinadini, M. van Loosdrecht and H. Younesi, A new anti-fouling polysulphone nanofiltration membrane blended by amine-functionalized MCM-41 for post treating waste stabilization pond's effluent, *J. Environ. Manag.*, 2021, **290**, 112649.

35 K. Sunil, P. Sherugar, S. Rao, C. Lavanya, G. R. Balakrishna, G. Arthanareeswaran and M. Padaki, Prolific approach for the removal of dyes by an effective interaction with polymer matrix using ultrafiltration membrane, *J. Environ. Chem. Eng.*, 2021, **9**(6), 106328.

36 B. Paulchamy, G. Arthi and B. D. Lignesh, A simple approach to stepwise synthesis of graphene oxide nanomaterial, *J. Nanomed. Nanotechnol.*, 2015, **6**(1), 1.

37 S. Sali, H. R. Mackey and A. A. Abdala, Effect of graphene oxide synthesis method on properties and performance of polysulfone-graphene oxide mixed matrix membranes, *Nanomaterials*, 2019, **9**(5), 769.

38 A. K. Shukla, J. Alam, M. Alhoshan, L. A. Dass and M. R. Muthumareeswaran, Development of a nanocomposite ultrafiltration membrane based on polyphenylsulfone blended with graphene oxide, Sci. Rep., 2017, 7(1), 1–12.

39 A. Spoială, C. I. Ilie, D. Ficai, A. Ficai and E. Andronescu, Chitosan-based nanocomposite polymeric membranes for water purification—A review, Materials, 2021, 14(9), 2091.

40 V. H. T. Nguyen, M. N. Nguyen, T. T. Truong, T. T. Nguyen, H. V. Doan and X. N. Pham, One-pot preparation of alumina-modified polysulfone-graphene oxide nanocomposite membrane for separation of emulsion-oil from wastewater, J. Nanomater., 2020, 2020, 1–12.

41 M. S. Alshammari, A. A. Essawy, A. M. El-Nggar and S. M. Sayyah, Ultrasonic-assisted synthesis and characterization of chitosan-graft-substituted polyanilines: promise bio-based nanoparticles for dye removal and bacterial disinfection, J. Chem., 2020, 2020, 1–9.

42 D. Ghernaout and A. El-Wakil, Requiring Reverse Osmosis Membranes Modifications—An Overview, Am. J. Chem. Eng., 2017, 5(4), 81–88.

43 R. Rezaee, S. Nasseri, A. H. Mahvi, R. Nabizadeh, S. A. Mousavi, A. Rashidi, A. Jafari and S. Nazmara, Fabrication and characterization of a polysulfone-graphene oxide nanocomposite membrane for arsenate rejection from water, J. Environ. Health Sci. Eng., 2015, 13, 1–11.

44 L. Badrinezhad, S. Ghasemi, Y. Azizian-Kalandaragh and A. Nematollahzadeh, Preparation and characterization of polysulfone/graphene oxide nanocomposite membranes for the separation of methylene blue from water, Polymer Bulletin, 2018, 75, 469–484.

45 A. Sarihan, Development of high-permeable PSf/PANI-PAMPSA composite membranes with superior rejection performance, Mater. Today Commun., 2020, 24, 101104.

46 D. Sharma and T. Singh, A DFT study of polyaniline/ZnO nanocomposite as a photocatalyst for the reduction of methylene blue dye, J. Mol. Liq., 2019, 293, 111528.

47 W. Li, Z. Xie, S. Xue, H. Ye, M. Liu, W. Shi and Y. Liu, Studies on the adsorption of dyes, Methylene blue, Safranin T, and Malachite green onto Polystyrene foam, Sep. Purif. Technol., 2021, 276, 119435.

48 M. Jamalludin, Z. Harun, M. Zakaria, W. Rahim, C. Khor, M. Rosli, M. Ishak, M. Nawi and S. Shahrin (2017), The effect of hydrophilicity of graphene oxide as additive towards performance of polysulfone membrane, 1885, AIP Conference Proceedings, pp. 020141.

49 H. Ravishankar, F. Roddick, D. Navaratna and V. Jegatheesan, Preparation, characterisation and critical flux determination of graphene oxide blended polysulfone (PSf) membranes in an MBR system, J. Environ. Manage., 2018, 213, 168–179.

50 A. Alkhouzaam and H. Qiblawey, Novel polysulfone ultrafiltration membranes incorporating polydopamine functionalized graphene oxide with enhanced flux and fouling resistance, J. Membrane Sci., 2020, 118900.

51 T. Kusworo, F. Dalanta, N. Aryanti and N. Othman, Intensifying separation and antifouling performance of PSf membrane incorporated by GO and ZnO nanoparticles for petroleum refinery wastewater treatment, J. Water Process Eng., 2021, 41, 102030.

52 X. Yuan, L. Wu, H. Geng, L. Wang, W. Wang, Y. Xueshuang, B. He, Y. Jiang, Y. Ning, Z. Zhu and J. Li, Polyaniline/polysulfone ultrafiltration membranes with improved permeability and anti-fouling behavior, J. Water Process Eng., 2021, 40, 101903.

53 S. Sontakke and V. Awate, The effect of synthesis parameters on the conductivity of PSf/PANI and PSf/PPy composite membranes, Can. J. Chem. Eng., 2018, 96, 564–572.

54 S. Teli, S. Molina, A. Sotto, E. García-Calvo and J. Abajob, Fouling Resistant Polysulfone–PANI/TiO$_2$ Ultrafiltration Nanocomposite Membranes, Ind. Eng. Chem. Res., 2013, 52, 9470–9479.

55 R. Damodar, S. You and S. Ou, Coupling of membrane separation with photocatalytic slurry reactor for advanced dye wastewater treatment, Sep. Purif. Technol., 2010, 76, 64–71.

56 N. Mokhtar, W. Lau, A. Ismail, W. Youravong, W. Khongnakorn and K. Lertwittayanon, Performance evaluation of novel PVDF–Cloisite 15A hollow fiber composite membranes for treatment of effluents containing dyes and salts using membrane distillation, RSC Adv., 2015, 5, 38011–38020.

57 F. Saravia, C. Zwiener and F. Frimmel, Interactions between membrane surface, dissolved organic substances and ions in submerged membrane filtration, Desalination, 2006, 192, 280–287.

58 C. Wei, Q. Cheng, L. Lin, Z. He, K. Huang, S. Ma and L. Chen, One-step fabrication of recyclable polyimide nanofiltration membranes with high selectivity and performance stability by a phase inversion-based process, J. Mater. Sci., 2018, 53, 11104–11115.

59 E. Steinle-Darling, M. Zedda, M. Plumlee, H. Ridgway and M. Reinhard, Evaluating the impacts of membrane type, coating, fouling, chemical properties and water chemistry on reverse osmosis rejection of seven nitrosoalkylamines, including NDMA, Water Res., 2007, 41(17), 3959–3967.

60 K. Kimura, R. Ogyu, T. Miyoshi and Y. Watanabe, Transition of major components in irreversible fouling of MBRs treating municipal wastewater, Sep. Purif. Technol., 2015, 142, 326–331.

61 S. Amiri, A. Asghari, V. Vatanpour and M. Rajabi, Fabrication and characterization of a novel polyvinyl alcohol-graphene oxide-sodium alginate nanocomposite hydrogel blended PES nanofiltration membrane for improved water purification, Sep. Purif. Technol., 2020, 250, 117216.

62 C. Lin, K. Tung, Y. Lin, C. Dong, C. Chen and C. Wu, Fabrication and modification of forward osmosis membranes by using graphene oxide for dye rejection and sludge concentration, Process Saf. Environ. Prot., 2020, 144, 225–235.

63 M. Marcucci, G. Nosenzo, G. Capannelli, I. Ciabatti, D. Corrieri and G. Ciardelli, Treatment and reuse of textile effluents based on new ultrafiltration and other membrane technologies, Desalination, 2001, 138, 75–82.

64 I. Ćurić, D. Dolar and J. Bošnjak, Reuse of textile wastewater for dyeing cotton knitted fabric with hybrid treatment:

coagulation/sand filtration/UF/NF-RO, *J. Environ. Manage.*, 2021, **295**, 113133.

65 W. Wang, Q. Bai, T. Liang, H. Bai and X. Liu, Two-sided surface oxidized cellulose membranes modified with PEI: preparation, characterization and application for dyes removal, *Polymers*, 2017, **9**(9), 455.

66 H. Ouaddari, A. Karim, B. Achiou, S. Saja, A. Aaddane, J. Bennazha, I. E. El Hassani, M. Ouammou and A. Albizane, New low-cost ultrafiltration membrane made from purified natural clays for direct Red 80 dye removal, *J. Environ. Chem. Eng.*, 2019, **7**(4), 103268.

67 T. T. Nguyen, T. K. Phung, X. T. Bui, V. D. Doan, T. Van Tran, K. T. Lim and T. D. Nguyen, Removal of cationic dye using polyvinyl alcohol membrane functionalized by D-glucose and agar, *J. Water Proc. Eng.*, 2021, **40**, 101982.

68 N. Neethu and T. Choudhury, Treatment of methylene blue and methyl orange dyes in wastewater by grafted titania pillared clay membranes, *Recent Pat. Nanotechnol.*, 2018, **12**(3), 200–207.